An Analogue Approach to Identify Heavy Precipitation Events: Evaluation and Application to CMIP5 Climate Models in the United States

Citation: Gao, Xiang, C. Adam Schlosser, Pingping Xie, Erwan Monier, and Dara Entekhabi. "An Analogue Approach to Identify Heavy Precipitation Events: Evaluation and Application to CMIP5 Climate Models in the United States." J. Climate 27, no. 15 (August 2014): 5941–5963. © 2014 American Meteorological Society

As Published: http://dx.doi.org/10.1175/jcli-d-13-00598.1

Publisher: American Meteorological Society

Persistent URL: http://hdl.handle.net/1721.1/95748

Version: Final published version: final published article, as it appeared in a journal, conference proceedings, or other formally published context

An Analogue Approach to Identify Heavy Precipitation Events: Evaluation and Application to CMIP5 Climate Models in the United States

XIANG GAO AND C. ADAM SCHLOSSER

Joint Program on the Science and Policy of Global Change, Massachusetts Institute of Technology, Cambridge, Massachusetts

PINGPING XIE

NOAA/Climate Prediction Center, College Park, Maryland

ERWAN MONIER

Joint Program on the Science and Policy of Global Change, Massachusetts Institute of Technology, Cambridge, Massachusetts

DARA ENTEKHABI

Department of Civil and Environmental Engineering, Massachusetts Institute of Technology, Cambridge, Massachusetts

(Manuscript received 1 October 2013, in final form 1 April 2014)

ABSTRACT

An analogue method is presented to detect the occurrence of heavy precipitation events without relying on modeled precipitation. The approach is based on using composites to identify distinct large-scale atmospheric conditions associated with widespread heavy precipitation events across local scales. These composites, exemplified in the south-central, midwestern, and western United States, are derived through the analysis of 27-yr (1979–2005) Climate Prediction Center (CPC) gridded station data and the NASA Modern-Era Retrospective Analysis for Research and Applications (MERRA). Circulation features and moisture plumes associated with heavy precipitation events are examined. The analogues are evaluated against the relevant daily meteorological fields from the MERRA reanalysis and achieve a success rate of around 80% in detecting observed heavy events within one or two days. The method also captures the observed interannual variations of seasonal heavy events with higher correlation and smaller RMSE than MERRA precipitation. When applied to the same 27-yr twentieth-century climate model simulations from Phase 5 of the Coupled Model Intercomparison Project (CMIP5), the analogue method produces a more consistent and less uncertain number of seasonal heavy precipitation events with observation as opposed to using model-simulated precipitation. The analogue method also performs better than model-based precipitation in characterizing the statistics (minimum, lower and upper quartile, median, and maximum) of year-to-year seasonal heavy precipitation days. These results indicate the capability of CMIP5 models to realistically simulate large-scale atmospheric conditions associated with widespread local-scale heavy precipitation events with a credible frequency. Overall, the presented analyses highlight the improved diagnoses of the analogue method against an evaluation that considers modeled precipitation alone to assess heavy precipitation frequency.

1. Introduction

Flooding associated with heavy precipitation is among the most disruptive weather-related hazards for the environment and the economy (Kunkel et al. 1999; Mass et al. 2011). In particular, there is concern that anthropogenic global warming could potentially increase the frequency and intensity of heavy precipitation events (Groisman et al. 2005; Palmer and Räisänen 2002; Kunkel et al. 2003). Such an increase, which has already been seen over the late twentieth century, would have substantial implications for public safety, water resource management, and other significant societal issues.

Climate models are useful tools for understanding and predicting changes in precipitation characteristics. However, previous studies have shown that global

Corresponding author address: Xiang Gao, E19-411h, MIT, 50 Ames St., Cambridge, MA 02139.
E-mail: xgao304@mit.edu

DOI: 10.1175/JCLI-D-13-00598.1

climate models in general do not correctly reproduce the frequency distribution of precipitation, especially at the regional scale. Dai (2006) and Sun et al. (2006) evaluated the performances of 18 coupled global climate models in simulating precipitation characteristics for the current climate. They found that most models overestimate the frequency of light precipitation, but considerably underestimate the frequency of heavy precipitation. Kharin et al. (2007) demonstrated that simulated present-day precipitation extremes from 14 Intergovernmental Panel on Climate Change (IPCC) Fourth Assessment Report (AR4) global coupled climate models are fairly consistent in the moderate and high latitudes but much less so in the tropics and subtropical regions. Wehner et al. (2010) showed that 20-yr return values of the annual maximum daily precipitation totals are severely underestimated at the typical resolutions of the coupled general circulation models over the continental United States. These studies suggest that there exist some model biases in the simulation of heavy precipitation statistics, despite differences regarding the models and observations used, geographical domain analyzed, and quantitative methods employed. Such biases were also found in high-resolution regional models. Gutowski et al. (2003) showed that a regional climate model overestimates low-density precipitation events but underestimates high-density precipitation events for a central U.S. region. Wehner (2013) examined the ensemble of North American Regional Climate Change Assessment Program (NARCAPP) regional climate models driven by National Centers for Environmental Prediction (NCEP) reanalysis and found that most of the models are biased high in the seasonal 10-yr return values averaged over the eastern and western U.S. regions.

Heavy precipitation often results from the interaction of synoptic-scale atmospheric features (i.e., moisture flow and dynamical instabilities) and local phenomena (i.e., terrain and other surface features). Lack of skill in climate models' regional distributions of precipitation is influenced by inadequate parameterization and/or representation of vertical motions, cloud microphysical processes, convection, and orography at the native grid scale of climate models. On the other hand, it has been shown that climate models do simulate fairly realistic large-scale atmospheric circulation features associated with heavy precipitation events, mostly because these features represent solutions of the common well-understood and numerically resolved equations. Hewitson and Crane (2006) demonstrated that precipitation downscaled from synoptic-scale atmospheric circulation changes in multiple GCMs can provide a more consistent projection of precipitation change than the GCM's precipitation. The regional climate models are also shown to be capable of reproducing the large-scale physical mechanisms associated with extreme precipitation over the Maritime Alps (Boroneant et al. 2006) and the upper Mississippi River basin region (Gutowski et al. 2008). Using the North American Regional Reanalysis (NARR), DeAngelis et al. (2013) evaluated the climate model simulations of daily precipitation statistics and the large-scale physical mechanisms associated with extreme precipitation from phase 3 of the Coupled Model Intercomparison Project (CMIP3) over North America. They found that robust biases exist in intensity of heavy and extreme precipitation among the models. However, the models were found to capture the large-scale physical mechanisms linked to extreme precipitation realistically, although the strength of the associated atmospheric circulation features tends to be overestimated. These results suggest that circulation analyses may give more robust indication of the occurrence and change in heavy precipitation events than simulated precipitation alone.

Multiple efforts have been made to identify distinct large-scale dynamical conditions (also known as composites) inducing local-scale extremes (Rudari et al. 2004; Rudari et al. 2005; Grotjahn 2011; DeAngelis et al. 2013), where the development of the composites is generally achieved by conditioning atmospheric reanalysis synoptic flows and fluxes on the occurrence of extreme events identified from local surface station observations. Such an approach bridges the scale gap between resolved large-scale features and heavy precipitation in localized regions that are smaller than the coarse resolution of the reanalysis data. In addition, the composites are based on a pooled set of extreme events that form a representative set of associated atmospheric conditions. Our work builds on and expands upon the heritage of previous studies. First, we construct composites of the distinct synoptic patterns associated with widespread localized heavy precipitation through the joint analysis of finescale surface precipitation observations and coarse-grid atmospheric reanalysis data. We then build a set of diagnostics to characterize these composites as an analogue for heavy precipitation events. We use these diagnostics to evaluate the daily reanalysis atmospheric fields against the composites and assess the success rate of the analogue approach to identify the observed heavy precipitation events. Finally, we examine the performances of this analogue approach in detecting the occurrence of heavy precipitation events when applied to the state-of-the-art climate model simulations against the observations and model-simulated precipitation. Our objectives are to answer such questions as follows: Can this analogue approach based on relevant large-scale atmospheric features provide useful skill in characterizing the statistics of heavy precipitation

frequency? How does its performance compare with observations and previous assessments based mostly on precipitation from model simulations and reanalysis? Is the approach robust enough to be applicable to various regions with similar performances? Here we present a prototype intended to address these questions.

The structure of the paper is as follows: In section 2, we describe the datasets (observations, reanalysis, and climate model simulations) used in this study. The observed precipitation statistics over the United States are given in section 3. In section 4, the procedure for determining the heavy precipitation events widespread at local scale is presented. Section 5 describes the composites of large-scale atmospheric conditions associated with widespread localized heavy events over our various study regions. We also introduce a set of diagnostics that serves as the foundation for using the composite analogues to identify the occurrence of heavy precipitation events based upon the analysis of daily atmospheric fields. The evaluation of the analogue approach is presented in section 6. The application of the analogue approach to the CMIP5 historical climate model simulations is presented and discussed in section 7. A summary and conclusions are provided in section 8.

2. Datasets

a. Observed precipitation

High-quality observations of accumulated daily precipitation were obtained from the National Oceanic and Atmospheric Administration (NOAA)/Climate Prediction Center (CPC) unified rain gauge-based analysis (Higgins et al. 2000b). These observations, spanning from 1948 to the present, are confined to the continental United States land areas and gridded to a 0.25° × 0.25° resolution from roughly 10 000 daily station reports. The analysis was produced using an optimal interpolation scheme and went through several types of quality control including ''duplicate station'' and ''buddy'' checks, among others. Previous assessments of gridded analyses and station observations over the United States have shown that gridded analyses are reliable for studies of fluctuations in daily precipitation as long as the station coverage is sufficiently dense and rigorous quality-control procedures are applied to the daily data (Higgins et al. 2007). Nevertheless, the station density and its change over time as well as missing data are sources of uncertainty in the analysis. The percentage of missing days at any grid cell is usually no more than 0.5% over the entire period, and therefore the missing data should not impact the results presented here. For the purposes of this exercise, the gridded daily analysis is used.

b. NASA MERRA reanalysis

Modern-Era Retrospective Analysis for Research and Applications (MERRA; Rienecker et al. 2011) was used to build the composites of large-scale atmospheric circulations associated with the localized heavy precipitation and to evaluate the analogue method. The MERRA uses the Goddard Earth Observing System Model, version 5 (GEOS-5) atmospheric circulation model, the Catchment land surface model, and an enhanced three-dimensional variational data assimilation (3DVAR) analysis algorithm. The data assimilation system of GEOS-5 implements the incremental analysis updates (IAU) procedure in which the analysis correction is applied to the forecast model states gradually. This has ameliorated the spin-down problem with precipitation and greatly improved aspects of stratospheric circulation. MERRA physical parameterizations have also been enhanced so that the shock of adjusting the model system to the assimilated data is reduced. In addition, MERRA incorporates observations from NASA Earth Observing Systems (EOS) satellites, particularly those from EOS/*Aqua*, in its assimilation framework. The MERRA is updated in real time, spanning the period from 1979 to the present. The three-dimensional 3-hourly atmospheric diagnostics on 42 pressure levels are available at a 1.25° resolution.

c. Climate model simulations

The climate model simulations used in this study were historical runs from the CMIP5 collection. These simulations were forced with observed temporal variations of anthropogenic and natural forcings and, for the first time, time-evolving land cover (Taylor et al. 2012). The historical runs cover much of the industrial period (from the mid-nineteenth century to near present) and are sometimes referred to as twentieth-century simulations. The climate models that we analyze are listed in Table 1 together with their horizontal grid resolutions and the number of vertical levels in the corresponding atmospheric components. Model output is available on a variety of horizontal resolutions and vertical levels. There are 20 models with sufficient daily meteorological variables for the analogue method to be applied. Because of the limited availability of multiple ensemble members, only one twentieth-century ensemble member run is analyzed from each model.

d. Data processing

The same set of meteorological variables associated with heavy precipitation events are compiled and analyzed from the MERRA reanalysis and climate model simulations, including 500-hPa height, 500-hPa vertical velocity, 500-hPa vector wind, 850-hPa vector wind, sea

TABLE 1. List of the CMIP5 models used for analysis in this study.

Model acronym	Climate model	Country	Resolution	Run	Institution
ACCESS1.0	Australian Community Climate and Earth-System Simulator, version 1.0	Australia	192 × 144L38	1	Commonwealth Scientific and Industrial Research Organization, and Bureau of Meteorology
ACCESS1.3	Australian Community Climate and Earth-System Simulator, version 1.3	Australia	192 × 144L38	1	Commonwealth Scientific and Industrial Research Organization, and Bureau of Meteorology
BCC_CSM1.1	Beijing Climate Center, Climate System Model, version 1.1	China	128 × 64L26	1	Beijing Climate Center, China Meteorological Administration
BCC_CSM1.1-m	Beijing Climate Center, Climate System Model, version 1.1-m	China	320 × 160L26	1	Beijing Climate Center, China Meteorological Administration
BNU-ESM	Beijing Normal University—Earth System Model	China	128 × 64L26	1	College of Global Change and Earth System Science, Beijing Normal University
CanESM2	Second Generation Canadian Earth System Model	Canada	128 × 64L35	5	Canadian Centre for Climate Modeling and Analysis
CCSM4	Community Climate System Model, version 4	United States	288 × 192L26	1	National Center for Atmospheric Research
CMCC-CM	Centro Euro-Mediterraneo sui Cambiamenti Climatici Climate Model	Italy	480 × 240L31	1	Centro Euro-Mediterraneo sui Cambiamenti Climatici
CNRM-CM5	Centre National de Recherches Météorologiques Coupled Global Climate Model, version 5	France	256 × 128L31	1	Centre National de Recherches Meteorologiques
GFDL-CM3	Geophysical Fluid Dynamics Laboratory Climate Model, version 3	United States	144 × 90L48	1	Geophysical Fluid Dynamics Laboratory
GFDL-ESM2G	Geophysical Fluid Dynamics Laboratory Earth System Model with Generalized Ocean Layer Dynamics (GOLD) component	United States	144 × 90L24	1	Geophysical Fluid Dynamics Laboratory
GFDL-ESM2M	Geophysical Fluid Dynamics Laboratory Earth System Model with Modular Ocean Model 4 (MOM4) component	United States	144 × 90L24	1	Geophysical Fluid Dynamics Laboratory
IPSL-CM5A-LR	L'Institut Pierre-Simon Laplace Coupled Model, version 5A, coupled with NEMO, low resolution	France	96 × 96L39	6	L'Institut Pierre-Simon Laplace
IPSL-CM5A-MR	L'Institut Pierre-Simon Laplace Coupled Model, version 5A, coupled with NEMO, mid resolution	France	144 × 143L39	3	L'Institut Pierre-Simon Laplace
IPSL-CM5B-LR	L'Institut Pierre-Simon Laplace Coupled Model, version 5B, coupled with NEMO, low resolution	France	96 × 96L39	1	L'Institut Pierre-Simon Laplace
MIROC5	Model for Interdisciplinary Research on Climate, version 5	Japan	256 × 128L40	5	Atmosphere and Ocean Research Institute, National Institute for Environmental Studies, and Japan Agency for Marine-Earth Science and Technology

TABLE 1. (*Continued*)

Model acronym	Climate model	Country	Resolution	Run	Institution
MIROC-ESM-CHEM	Model for Interdisciplinary Research on Climate, Earth System Model, Chemistry Coupled	Japan	128 × 64L80	1	Japan Agency for Marine-Earth Science and Technology, Atmosphere and Ocean Research Institute, and National Institute for Environmental Studies
MIROC-ESM	Model for Interdisciplinary Research on Climate, Earth System Model	Japan	128 × 64L80	3	Japan Agency for Marine-Earth Science and Technology, Atmosphere and Ocean Research Institute, and National Institute for Environmental Studies
MRI-CGCM3	Meteorological Research Institute Coupled Atmosphere–Ocean General Circulation Model, version 3	Japan	320 × 160L48	1	Meteorological Research Institute
NorESM1-M	Norwegian Earth System Model, version 1 (intermediate resolution)	Norway	144 × 96L26	3	Norwegian Climate Centre

level pressure, precipitable water, and vertically integrated water vapor flux. CMIP5 climate models do not provide precipitable water and vertically integrated water vapor flux as direct output. These two variables are derived from the vector wind, specific humidity, and surface air pressure with the integration performed from surface to 30 hPa (midway between the last two pressure levels). The vertically integrated water vapor flux is indicative of the magnitude of moisture transport feeding heavy precipitation events in local areas. The more relevant diagnostic is vapor convergence. Unfortunately, the estimate of vertically integrated vapor convergence based on reanalysis is problematic as a result of the required total mass balance correction. The vertically integrated water vapor flux, though limited, provides the main basis for qualitatively identifying the distinct patterns in moisture transport toward the localized heavy hydrometeorological events.

The precipitation and meteorological fields from MERRA reanalysis and each CMIP5 climate model are all regridded to the common 2.5° × 2° resolution via linear interpolation if the original climate model resolution is coarser than that of the target resolution or area averaging otherwise. All of the atmospheric quantities are converted to a standardized anomaly at each grid cell. The standardized anomaly is defined as the anomaly from the seasonal climatological mean over the 27-yr period divided by the standard deviation. Expressing the data in terms of standardized anomalies allows comparison and aggregation between data with different variabilities and means. The time period with the greatest overlap among the CPC observations, MERRA, and CMIP5 models is 1 January 1979–31 December 2005, so all of the following analyses are made for this 27-yr period.

We use the CPC observed precipitation to identify the heavy precipitation events at local scale, while the MERRA reanalysis is used to construct the large-scale composites of atmospheric patterns associated with heavy precipitation. The presented analogue approach is mainly for characterizing the frequency of a class of heavy precipitation events (e.g., the top 5%). It should be noted that, when applying this method to the CMIP5 historical simulations, a reproduction of the exact date when heavy precipitation event occurs is not expected, in large part because of the limits of deterministic predictability of atmosphere (Lorenz 1965). Rather, the intent of this procedure is to examine the collective performances of the CMIP5 models in detecting the cumulative occurrence of the heavy precipitation events—over a given spatial and temporal domain of interest—based on derived large-scale physical mechanisms and how such analogue approach compares with observations and traditional model-simulated precipitation.

3. Observed precipitation statistics

a. Definition of heavy precipitation

Three different methods have been commonly used to identify heavy precipitation events. The first method is based on the actual rainfall amounts. For example, a ''heavy'' rainfall climatology is constructed as daily precipitation exceeding 50.8 mm (2 inches) and a ''very

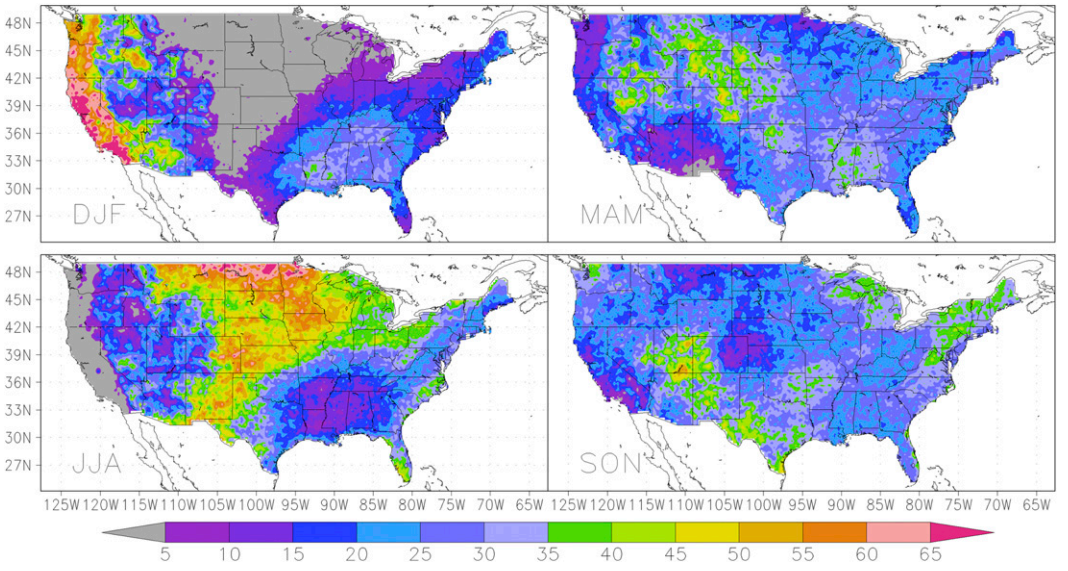

FIG. 1. The percentage of heavy precipitation events that occur in each season (DJF, MAM, JJA, and SON) over the contiguous United States.

heavy'' rainfall climatology exceeds 101.6 mm (4 inches) (Groisman et al. 1999). A second way is to use specific thresholds such as the 95th and 99th percentiles of precipitation frequency distribution for heavy and very heavy events, respectively. Estimation of the percentiles is generally based on days with precipitation excluding days without precipitation (Groisman et al. 2001; Klein Tank et al. 2009). A third way is to calculate return values for specified return periods based on the seasonal or annual maximum daily precipitation series (Kunkel et al. 1999), which is typically used for risk analysis. In a complex orography environment, differences in elevation over short distances can lead to dramatic changes in precipitation distribution owing to the interaction of topography and atmospheric flows. As such, defining heavy precipitation based on daily accumulation amount could be problematic in this context. In this study, we define a precipitation event as daily precipitation above 1 mm day^{-1} recorded at one observational or model grid. A heavy precipitation event is hereafter defined as the daily precipitation amount exceeding the 95th percentile of all precipitation events during a specific period (season).

b. Regional and seasonal considerations

Because seasonality strongly affects the dominant features of heavy precipitation and precipitation climatology in a specific region, we first examine the season and region to focus our analysis on. Figure 1 shows the percentage of heavy precipitation events occurring in each season over the contiguous United States. This is obtained by binning all of the top 5% precipitation events of the entire time series into each season at each grid cell, which reveals the season when heavy precipitation events are most frequent over the specific region. As shown in Fig. 1, heavy precipitation events over the West Coast mostly occur in the winter season [December–February (DJF)] with more than 60% of the events, while less than 5% of heavy events occur in the summer season [June–August (JJA)]. The other two seasons [March–May (MAM) and September–November (SON)] share almost the same number of remaining events, except that the autumn season (SON) is more populated than spring over Washington and Oregon. The contrasting characteristics over the midwestern United States are immediately evident. Heavy events dominates mostly in the summer season with more than 50%, while the winter season contains less than 5% of events. Also evident is that over the south-central United States three seasons (DJF, MAM, and SON) exhibit the equally dominant percentage of heavy events, while the summer season (JJA) indicates the least importance.

Figure 2 shows the 95th percentile of precipitation events (>1 mm day^{-1}) for each season over the contiguous United States. The most striking aspect is the sharp division between east and west. There exist large differences in the magnitudes, usually ranging from 5 to 50 mm day^{-1}. Also evident is the seasonality exhibited by these heavy events. In much of coastal western United States, the winter season shows the largest values of 50 mm day^{-1} above and exhibits a dependence on orography. Such high value can also be observed in some scattered areas in the spring and autumn seasons.

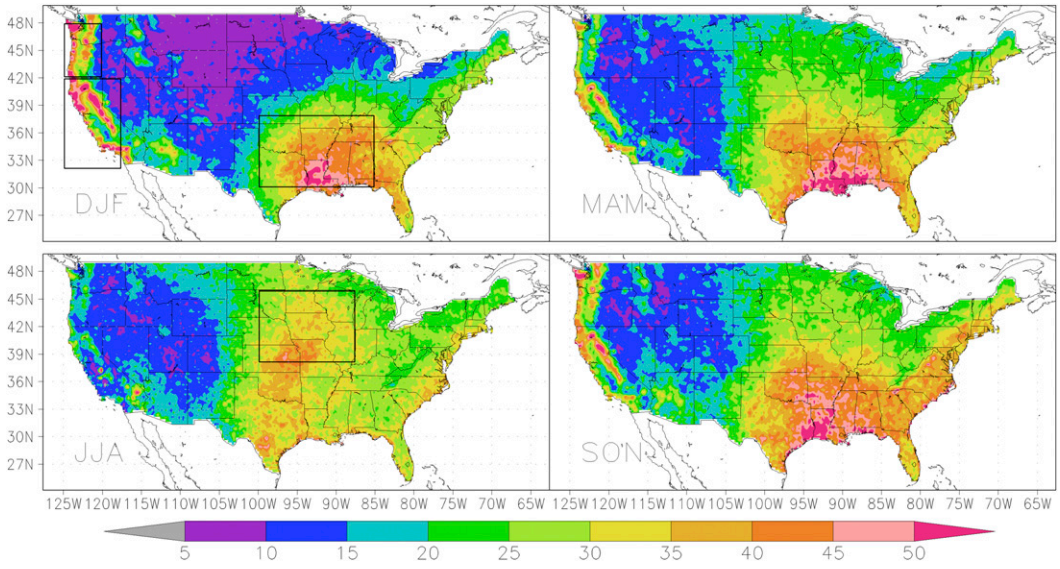

FIG. 2. The 95th percentile (mm day^{-1}) of precipitation events (>1 mm day^{-1}) for each season over the contiguous United States. The black rectangles indicate four regions examined in this study: the south-central United States, the midwestern United States, and the northern and southern flanks of the Pacific coast.

Conversely, the summer season is usually characterized with little precipitation and the smallest values of 5–15 mm day^{-1}. In the upper U.S. Midwest, the situation is reversed with the largest magnitudes (>35 mm day^{-1}) occurring in the summer, whereas the 95th percentiles in the winter season are usually less than 15 mm day^{-1}. Over the mountain west (or the interior west), 95th percentiles reveal much less variability among the seasons with the magnitude mostly less than 15 mm day^{-1}. In the southeast United States, all three seasons (DJF, MAM, and SON) exhibit consistently high 95th percentile values, mostly in the range of 35–50 mm day^{-1}. Heavy precipitation of this severity in the autumn (SON) is probably associated with Atlantic hurricane activity, while the source of winter (DJF) and spring (MAM) heavy precipitation is likely from severe storms moving across the midcontinent. The summer season is usually involved with much lighter precipitation except for eastern Texas and Oklahoma. These features are consistent with what is shown in Fig. 1.

c. *Study area*

We focus our analysis on regions where the seasonal precipitation is likely affected by synoptic-scale atmospheric patterns. Three such regions show salient features in this context: the south-central United States (SCUS), the midwestern United States (MWST), and the Pacific coast. The SCUS domain is defined as a window bounded by 30.125°–37.875°N, 99.875°–85.125°W for the 0.25° × 0.25° resolution (31°–37°N, 98.75°–86.25°W for the 2.5° × 2° resolution), including the states of Texas, Oklahoma, Louisiana, Arkansas, Mississippi, Tennessee, and Alabama. Higgins et al. (2011) suggest that a large number of localized heavy rain events lead to major flooding across portions of the SCUS. The heavy precipitation events in the SCUS exhibit the characteristics of the "Maya Express" flood events that link tropical moisture from the Caribbean and Gulf of Mexico to midlatitude flooding over the central United States (Higgins et al. 2011). Based on observed precipitation statistics, both winter (DJF) and spring (MAM) seasons are analyzed, but only the results for DJF are shown, as the MAM results are quite similar. For the midwestern United States, we focus on the northern U.S. Great Plains, especially a region bounded by 38.125°–45.875°N, 99.875°–87.625°W for the 0.25° × 0.25° resolution (39°–45°N, 98.75°–88.75°W for the 2.5° × 2° resolution), including the states of Kansas, Missouri, Nebraska, Iowa, Illinois, South Dakota, Minnesota, and Wisconsin. This region is chosen because it represents the area that is prone to widespread flooding events. Dirmeyer and Kinter (2010) demonstrated that flood cases in the U.S. Midwest are often associated with an anomalous transport of moisture from the subtropics or tropics, originating as evaporation from the Gulf of Mexico, eastern Mexico, or in particular the Caribbean Sea. This fetch of Caribbean moisture, also characteristics of the Maya Express, links into the Great Plains low-level jet, creating a much longer "atmospheric river" of moisture. They further stated that the period from May to July is not dominated by intense tropical cyclone activity and the low-latitude moisture is mainly

carried northward into the Midwest by the general circulation. Based on this fact and the observed precipitation characteristics, the June–August period is analyzed. The Pacific coast is a typical region where large-scale flows and complex topography are contributing factors to the occurrence of heavy precipitation events. The causes of West Coast heavy precipitation events are rather complex because multiple time scales are usually involved. The observed precipitation statistics indicates that heavy precipitation events occur most frequently in the winter season (DJF) with the largest 95th percentile. Studies have demonstrated that precipitation areas of major events along the Pacific coast are mostly associated with atmospheric rivers or the ''Pineapple Express'' that fetches moisture from the oceans around Hawaii during wet winters (Higgins et al. 2000a; Warner et al. 2012). We focus on the wintertime heavy precipitation events and further divide the Pacific coast into north coast [Washington and Oregon (WAOR)] and south coast [California (PCCA)]. The domain for WAOR is defined as a window (42.125°–47.875°N, 124.875°–120.125°W for the 0.25° × 0.25° resolution; 43°–47°N, 123.75°–121.25°W for the 2.5° × 2° resolution). The domain for PCCA is defined as a window (42.125°–47.875°N, 124.875°–117.625°W for the 0.25° × 0.25° resolution; 33°–41°N, 123.75°–118.75°W for the 2.5° × 2° resolution). Figure 2 depicts the location of the regions referenced in this study. The boundary of each domain at the fine and coarse resolution is defined to ensure the same area coverage.

4. Identification of localized widespread heavy precipitation events

Over any grid within each domain of interest, we extract the top 5% of all precipitation events in the season of our interest (DJF or JJA) as heavy daily events for that season. From these events, we examine two schemes to determine widespread heavy precipitation events (and thus likely candidates for synoptic-scale association). The first one employs a nonparametric bootstrap scheme that involves the random reshuffling of the entire seasonal precipitation time series at each grid within the domain. The bootstrap scheme is repeated 100 times to ensure the statistical stability and robustness. Based on the resulting distributional behavior of the heavy events, we choose the number of heavy events (the number of 0.25° × 0.25° grid cells) occurring on the same day as a threshold above which there is only 5% chance that their occurrence can be explained by random process. The second scheme involves the assessment of the clustering of the heavy events occurring on the same day based on their geographical coordinates (latitude and longitude). The clustering requires that the heavy events adjoin one another by at least one neighbor. We examine the cutoff value for the size of clustered events by comparing with the top 5% precipitation events identified from observations regridded to a 2.5° × 2° resolution. As expected, we find that the identified heavy events from observations at 0.25° × 0.25° in many cases coincide with but are much more than those from observations at 2.5° × 2°. In particular, as the cutoff value for the size of the clustering increases, the mismatch in the identified heavy events from two scales decreases. The cutoff value is chosen that a maximum 10% of mismatch cannot be exceeded. We find that the two schemes for determining widespread heavy precipitation events produce rather similar results. In the following sections, we only present the analyses from the bootstrap scheme. The procedure designates 44 or more simultaneous heavy events (on 44 or more equivalent 0.25° grid cells) as widespread events for SCUS, 40 for MWST, 26 for PCCA, and 23 for WAOR. This results in 345 days for SCUS, 570 days for MWST, 210 days for PCCA, and 284 days for WAOR in the DJF or JJA seasons of the 1979–2005 period.

5. Development of analogue method

The distinct large-scale meteorological patterns associated with heavy precipitation events are examined through the composites of various atmospheric variables from the MERRA reanalysis. Each composite is computed by averaging the relevant atmospheric variables on the set of dates with identified widespread heavy precipitation events for the domain of interest. Emphasis is placed on the circulation features and associated moisture plumes, including 500-hPa height, 500-hPa vertical velocity, total precipitable water, and the vertical integral of atmospheric vapor flux vectors. Sea level pressure and vector wind are also examined but not shown. We also attempt to assess whether the individual members used to construct these composites have any statistical distinction from the remaining members and therefore promise as predictive analogues.

a. Composites

Figures 3 and 4 show the composites of different variables as standardized anomalies for all the regions examined in this study. The composite of 500-hPa geopotential height (Z_{500}) for SCUS in DJF features a dipole pattern associated with a pronounced trough centered between the southwest and west south-central states and a ridge over the southeastern coast of the United States (Fig. 3a). Also evident are strong low-level flow (not shown) and moisture transport

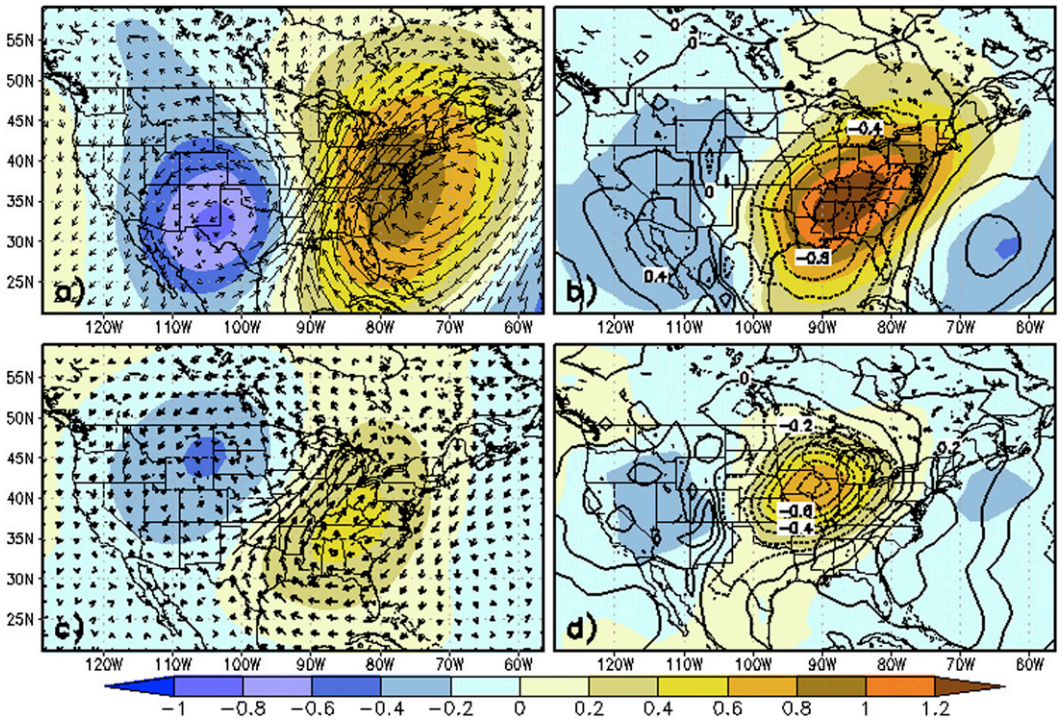

FIG. 3. Composite fields as standardized anomalies for the south-central United States in DJF: (a) 500-hPa geopotential height Z_{500} (shaded) and the vertical integral atmospheric vapor flux vector based on 345 widespread heavy precipitation events and (b) 500-hPa vertical velocity ω_{500} (contour) and total precipitable water (shaded). (c),(d) As in (a),(b), but for the midwestern United States in JJA based on 570 widespread heavy precipitation events.

(Fig. 3a) extending from the central Gulf of Mexico north-northeastward across the southeast and mid-Atlantic states. The origins of this moisture plume extends farther south and east toward the Caribbean Sea. Moister air [high precipitable water (TPW)] is clearly evident along the western edge of the geopotential ridge along the eastern United States (Fig. 3b). There also exists strong synoptic-scale upward motion (ω_{500}) over the Tennessee and Ohio valleys (Fig. 3b).

Figures 3c and 3d show the composites based on the 570 widespread heavy events identified for the midwestern United States (MWST) in the summer season (JJA). Compared with Figs. 3a and 3b, the relative strength is much weaker for all the meteorological fields. Nevertheless, we can still see that the 500-hPa circulation is characterized by negative height anomalies over the western United States, while weak positive height anomalies are observed over the eastern United States. The entire study region is situated downstream of the large-scale trough axis. Compared with the composites of the south-central United States, positive anomalies shift westward, while negative anomalies shift northward centered around the northwest mountain states. The moisture transport (Fig. 3c) can be seen extending from the central Gulf of Mexico north-northeastward across the north-central states. The origins of this moisture plume may extend farther south and east toward the Caribbean Sea. Moister air and strong synoptic-scale upward motion are also clearly observed, centered around our study region (Fig. 3d).

Figure 4 shows the same analyses but for the other two study regions in DJF. For the PCCA region (210 events), Z_{500} reveals the presence of distinctive negative height anomaly centered over the eastern North Pacific Ocean and the northwestern coast of the United States and weakened positive anomalies centered over the central Pacific (Fig. 4a). There is an anomalous southwesterly flow of moist air from the eastern North Pacific Ocean into the central western coast of the United States. Also evident are moister air and strong synoptic-scale upward motion centered over the northern California and Nevada but extending toward the interior western United States (Fig. 4b).

There is great resemblance between the composites for the WAOR region (284 events) and for the PCCA region, except that the centers of the anomalies shift slightly northward (Figs. 4c,d). The negative anomaly of Z_{500} is centered over the British Columbia coast and extends to the northwest over Alaska. The positive anomaly is centered near the Baja California Peninsula

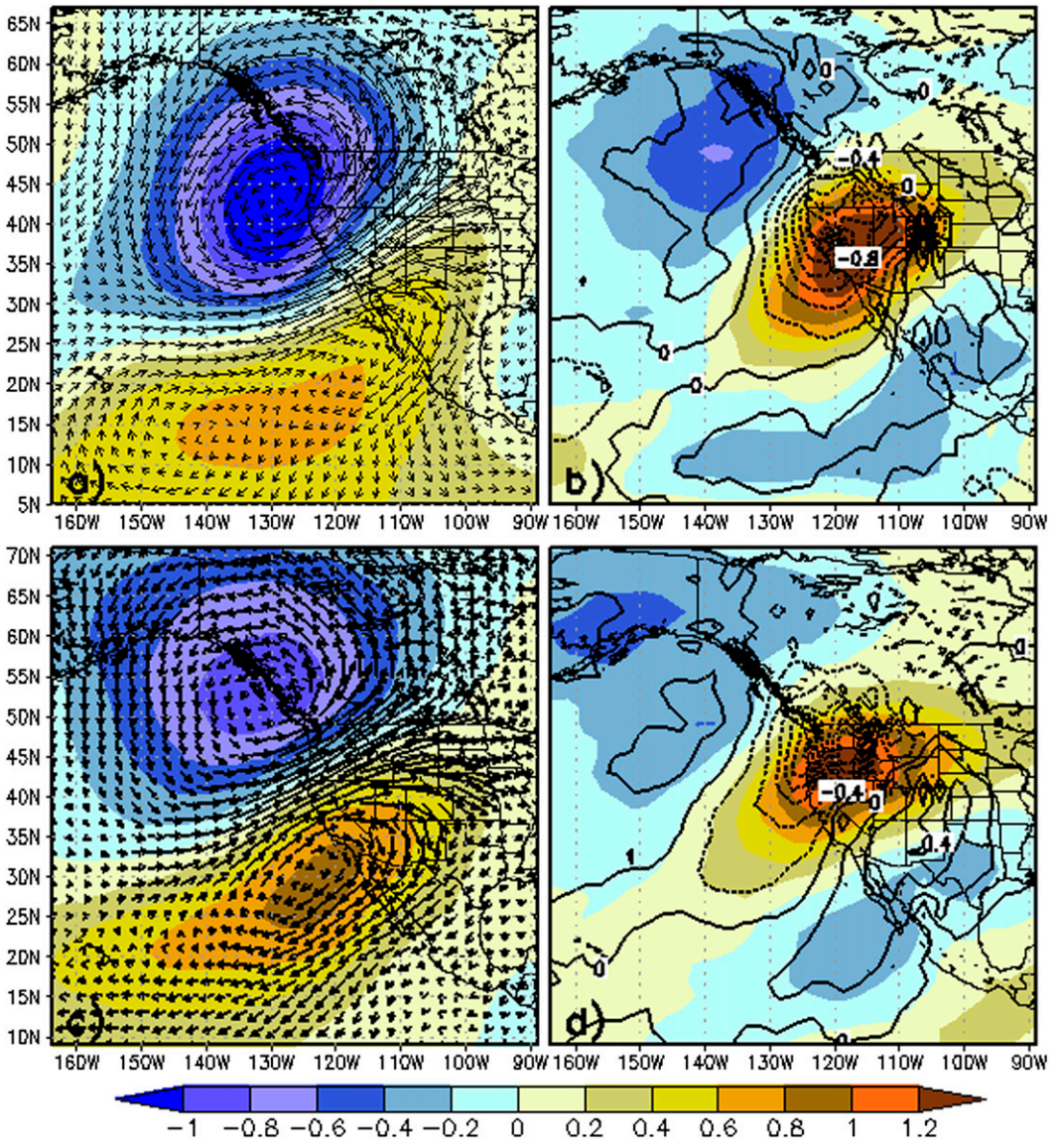

FIG. 4. Composite fields as standardized anomalies for the southern Pacific coast (California) in DJF: (a) 500-hPa geopotential height (shaded) and the vertical integral atmospheric vapor flux vector based on 210 widespread heavy precipitation events and (b) 500-hPa vertical velocity (contour) and total precipitable water (shaded). (c),(d) As in (a),(b), but for the northern Pacific coast (Washington and Oregon) in DJF based on 284 widespread heavy precipitation events.

and extends to the northeast over the interior western United States. Strong moisture transport extends from the eastern North Pacific Ocean northeastward across the northwestern United States. There exist also moister air and strong synoptic-scale upward motion directly over the study domain.

b. Analogue diagnostics

Based on the previously presented composites, we develop an analogue method that can be used to detect the occurrence of heavy precipitation events. This includes the assessment of collective characteristics for the individual members of the composites and the remaining members that are not used to construct the composites. The procedure is exemplified with the south-central United States and developed similarly for other three regions.

Following previous work (Grotjahn 2011), we examine how consistent the patterns are among the members of the composites by calculating sign counts at each grid cell (Fig. 5). Sign counts record the number of individual members whose standardized anomalies have

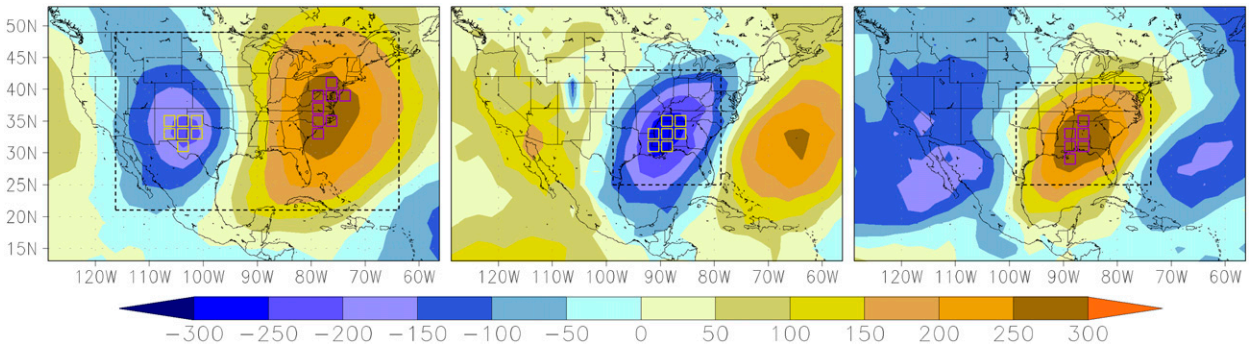

FIG. 5. (left)–(right) Sign counts of the composite members for Z_{500}, ω_{500}, and TPW as standardized anomalies over the SCUS. The highlighted grid cells indicate those with high sign consistency among the members of the composites (with large sign counts) and are used to construct the criteria of detection for the occurrence of heavy precipitation events. The dashed rectangles indicate the regions used to calculate the SACCs (see text for further details).

consistent sign with the composites. Positive (negative) sign counts correspond to consistently positive (negative) values among the members. If all the members have positive signs at a particular grid cell, the sign count at that grid would be the number of the identified widespread heavy events (i.e., 345 for the SCUS). Mostly some positive and negative anomalies would cancel out each other, resulting in smaller sign counts. It is evident that spatial patterns of the sign-count maps show strong consistency with the magnitudes of corresponding composite fields. Sea level pressure (SLP) is analyzed but not shown here. We then identify "hotspots" as a group of grid cells that are coherent among the members of the composites with regard to sign consistency: that is, cluster of grid cells with the largest sign counts (either positive or negative, see Fig. 5). The cutoff values for sign counts to determine the number of hotspot grid cells are chosen as 95% of relative maximum. One of the criteria for the occurrence of heavy precipitation events is the consistency in the sign of the daily meteorological variables (as standardized anomalies) from the climate models or reanalysis with that of the composites over the hotspot grid cells.

We further examine whether any statistical distinctions exist between the MERRA daily meteorological variables on the dates identified with heavy precipitation events and the other remaining dates. This is achieved by calculating the spatial anomaly correlation coefficients (SACCs) between the MERRA daily meteorological variables and the composites and comparing the SACC distributions from the dates with heavy precipitation events and the remaining dates. The location of the regions selected for SACC calculation is arbitrary, but are chosen to be centered around the hotspot grids (Fig. 5). Figure 6 shows the percent frequency distributions of the SACCs for the dates with heavy precipitation events and the remaining dates for the relevant meteorological fields. The vertical integral of atmospheric vapor flux vector is not analyzed here. The modes of the distributions for the remaining dates are immediately evident with more than 55% of the remaining dates having negative SACCs for all the meteorological variables, while less than 10% falls in other discrete intervals and less than 5% in the intervals larger than 0.4. As expected, the distributions for the pool of heavy precipitation events (which construct the composites) are populated toward higher SACCs. Although no single SACC value strongly dominates the distributions, the majority of the distributions lies in relatively higher SACCs for all meteorological variables as composed to the distributions for the remaining dates. For example, the SACCs larger than 0.3 account for about 80%, 80%, 60%, and 50% of the distributions for Z_{500}, SLP, TPW, and ω_{500}, respectively. In contrast, there are only 28%, 27%, 14%, and 13% for the distributions of the remaining dates. Nevertheless, there is no single SACC value at which two distributions can be clearly separable from each other. We define the thresholds to distinguish the two distributions as values for which percentages of the SACCs for the distribution of the remaining dates is less than 5% and percentages of the SACCs for the distribution of heavy precipitation events are more than double those for the remaining dates. This gives the thresholds of SACC larger than 0.5 for Z_{500} and larger than 0.3 for ω_{500} and TPW. SLP provides comparable information to Z_{500}, so it is not included in the following analyses. A limitation with SACCs is that their values will be dependent on the size of regions, as shown in Fig. 5. We examine the regions of different sizes to calculate the SACCs, but find that the two frequency distributions and the resulting thresholds remain essentially the same for all variables.

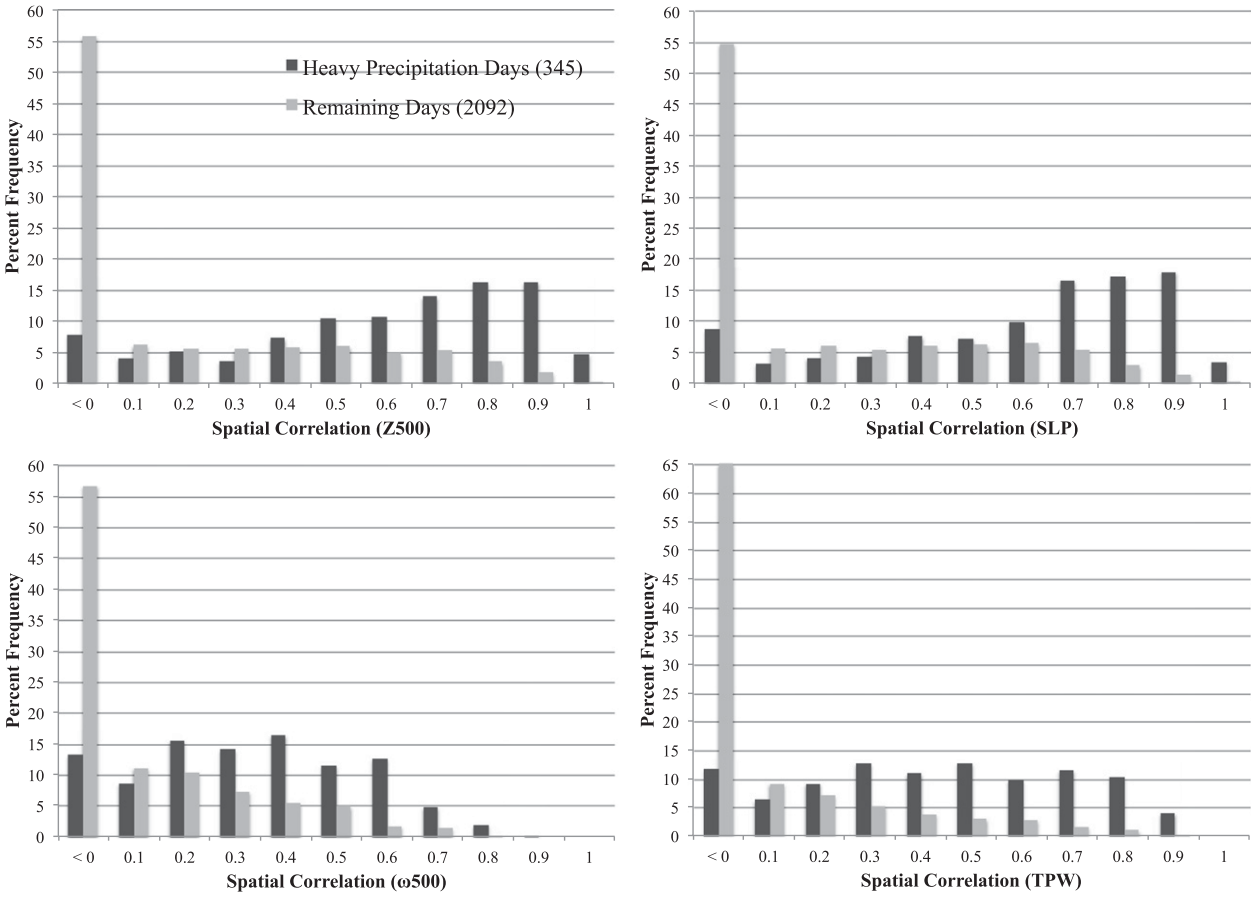

FIG. 6. Percent frequency distributions of the SACCs between the members (345) of the composites and the remaining members (2092) against the composites over the SCUS for Z_{500}, SLP, ω_{500}, and TPW.

We then construct a set of criteria for the occurrence of heavy precipitation events (''criteria of detection''). This is achieved by examining each member of the composites for the sign consistency over the hotspot grid cells and SACC values. We find that most of the members share the following common features: 1) At least 3 out of 4 variables (trough and ridge of Z_{500}, TPW, and ω_{500}) have consistent signs with the composites over selected hotspot grid cells; 2) at least 1 out of 3 variables (Z_{500}, TPW, and ω_{500}) has SACCs larger than the specified thresholds; and 3) all the SACCs have to be positive. These three conditions will serve as the criteria of detection for the analogue method. The predetermined cutoff values (noted above) for the sign counts and the SACCs thresholds are further refined before the criteria of detection are applied for event detection in climate model simulations. This refinement is performed such that the desired criteria of detection produce the approximate number of observed heavy precipitation events based on the entire span of MERRA daily meteorological fields for the given season. The selection of different individual or combinations of variable(s) to form the criteria for the analogue detection is also possible. The performances of these alternative choices in detecting the occurrence of observed heavy precipitation events are evaluated in section 6.

Sign counts and percent frequency distribution of SACCs are also examined for the MWST, PCCA, and WAOR. The hotspot grid cells are identified for each region. Similar criteria are employed to define the SACC thresholds that distinguish between the SACC distributions for the dates with heavy precipitation events and the remaining dates. For the MWST, the procedure results in the SACC values larger than 0.5 for Z_{500} and larger than 0.4 for ω_{500} and TPW as the thresholds. For the PCCA, the resulting SACC thresholds are larger than 0.6 for Z_{500} and larger than 0.4 for ω_{500} and TPW. WAOR has the thresholds of larger than 0.5 for Z_{500}, larger than 0.3 for ω_{500}, and larger than 0.4 for TPW. However, there exist some differences in the established criteria of detection for

TABLE 2. Evaluation with MERRA daily meteorological fields of skills of the analogue method in capturing observed heavy precipitation events based on various criteria over our study regions. The skills are expressed as success rate and false positive (see text for further details). Criteria of Z_{500}, ω_{500}, and TPW represent the selection of any single variable (trough or ridge of Z_{500}, ω_{500}, and TPW) to identify the occurrence of heavy precipitation events, respectively. Each variable should have consistent sign with its corresponding composite over the selected hotspot grid cells and also have its SACC value larger than the specified threshold. A reduced sample of two variables (RSAMP) is similar to the criteria of detection defined in section 5b, except that at least two (instead of three) out of four variables (trough and ridge of Z_{500}, TPW, and ω_{500}) have consistent signs with the corresponding composites over their selected hotspot grid cells. "Obs" and "MERRA-analogue" indicate the number of 27-yr seasonal heavy precipitation events based on the precipitation observation at 0.25° × 0.25° and the analogue method, respectively. The parenthesis shows the bias toward the observation.

Region	Criteria	Obs	MERRA-analogue (bias)	Success rate (%)			False positive (%)		
				Exact	±1 day	±2 days	Exact	±1 day	±2 days
SCUS	Criteria of detection	345	350 (5)	58.0	80.6	83.5	42.9	28.3	22.6
	Z_{500}		408 (63)	51.9	67.0	72.8	56.1	28.7	19.6
	ω_{500}		239 (−106)	29.9	48.7	54.5	56.9	49.4	43.5
	TPW		309 (−36)	47.3	71.0	76.2	47.3	34.3	28.5
	RSAMP		428 (83)	63.5	84.1	86.7	48.8	33.6	27.1
PCCA	Criteria of detection	210	221 (11)	61.4	78.1	80.5	41.6	29.0	20.4
	Z_{500}		337 (127)	53.3	66.2	71.9	66.8	46.6	36.5
	ω_{500}		180 (−30)	36.2	61.9	71.9	57.8	46.7	40.6
	TPW		251 (41)	59.1	77.1	81.0	50.6	38.3	32.3
	RSAMP		338 (128)	72.9	88.1	92.4	54.7	38.8	29.9
WAOR	Criteria of detection	284	277 (−7)	60.6	79.2	82.4	37.9	21.3	16.6
	Z500		344 (60)	55.3	67.3	73.2	54.4	27.3	18.0
	ω500		184 (−100)	43.7	68.0	73.6	32.6	17.9	15.2
	TPW		207 (−77)	40.9	64.4	70.1	44.0	31.4	24.6
	RSAMP		387 (103)	71.5	86.3	88.0	47.6	29.7	21.7
MWST	Criteria of detection	570	566 (−4)	56.7	78.1	85.8	42.9	22.8	15.6
	Z500		356 (−214)	32.3	44.4	50.9	48.3	19.1	10.4
	ω500		336 (−234)	31.8	55.6	65.6	46.1	28.9	22.3
	TPW		321 (−249)	31.9	52.8	62.8	43.3	29.0	21.5
	RSAMP		698 (128)	62.3	82.6	89.7	49.1	27.2	19.3

the MWST in JJA and for the other three regions in DJF. We notice that the atmospheric patterns are generally less consistent in their signs among the members of the composites in the MWST compared with in other regions. So, instead of using 95% of relative maximum as the cutoff values for the sign counts, only the grid with the maximum sign count is selected as a hotspot for each meteorological field. In addition, the SACC values of three variables do not have to be all positive.

6. Evaluation of analogue method

The criteria of detection established for each study region are evaluated with the 27-yr MERRA daily meteorological fields (500-hPa geopotential height, total precipitable water, and 500-hPa vertical velocity standardized anomalies) of specific season for the occurrences of heavy precipitation events (Table 2). For any particular day of the entire season, MERRA meteorological fields are evaluated against the constructed MERRA composites in terms of the sign consistency over the hotspot grids and the SACC values computed over the designated region shown in Fig. 5. If the criteria of detection are met, we consider the day as having a heavy precipitation event. We evaluate the performance of the analogue method as a success rate of detection and a false positive rate. The success is measured as the fraction (or percentage) of observed 27-yr seasonal heavy precipitation events that are also detected by the analogue method. The false positive is measured as the fraction (or percentage) of mistakenly identified heavy precipitation events by the analogue method. The success rate of the criteria of detection in matching the exact dates of the heavy precipitation events can reach about 57%–61% across four study regions. The results improve to 78%–80% and 81%–86% if the window for matching dates is enlarged to ±1 and ±2 days, respectively. The increases in success rate are large when the matching window is enlarged to ±1 day but start to level off for the matching window of ±2 days. Accordingly, the false positive rate is reduced from 21%–29% to 16%–23%. When compared with a reduced sample of any one or two variables (trough and ridge of Z_{500}, TPW, and ω_{500}), the criteria of detection are shown to achieve the best combination of success and false positive rates.

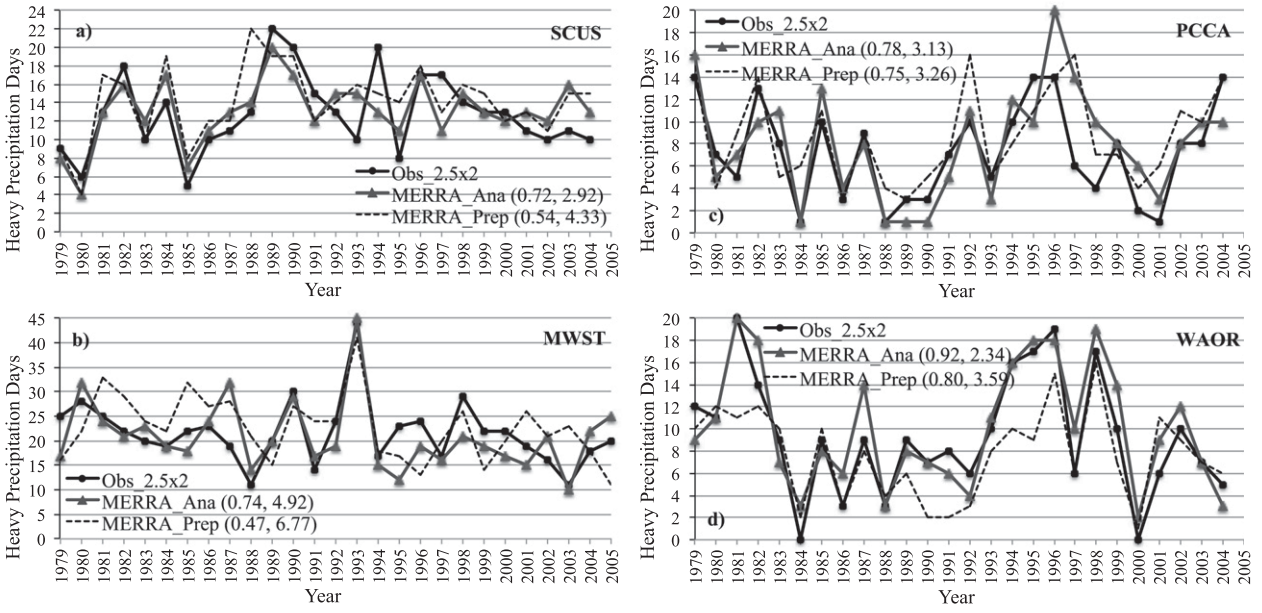

FIG. 7. Comparisons of interannual variations of seasonal heavy precipitation frequency obtained from the observation at 2.5° × 2° (Obs_2.5×2), MERRA precipitation (MERRA_Prep), and MERRA analogue method (MERRA_Ana) for all the study regions. The MERRA analogue results are obtained by evaluating the 27-yr MERRA daily meteorological fields of specific seasons based on the established criteria of detection. Also shown in the parentheses of the figure legends are temporal correlations and RMSE between the MERRA analogue method as well as MERRA precipitation against the observation.

Although a reduced sample of two variables (RSAMP) performs rather well with the highest success rate, it also produces a higher false positive rate than the criteria of detection. In addition, such high success rate is mostly compromised by the large biases in the total number of detected heavy precipitation occurrence. This is evidently expected: as the number of the ''tagged'' occurrence increases, the chance of success increases. These results indicate that the climate analogue method based on the constructed criteria of detection achieves the most robust results in detecting the occurrence of heavy precipitation events within ±2 days with satisfactory performances across various regions examined in this study.

We further examine the performance of the analogue method in depicting the interannual variations of seasonal heavy precipitation frequency as opposed to the precipitation observation aggregated to 2.5° × 2° and MERRA precipitation (2.5° × 2°) for all the study regions (Fig. 7). A heavy precipitation event from any type of precipitation data at 2.5° × 2° (observations, MERRA reanalysis, and CMIP5 models) is defined as the daily precipitation amount exceeding the 95th percentile of all precipitation events during a specific season at any data grid within the region of interest. For the DJF season, the number of heavy precipitation days for each year is computed based on the numbers in December of the current year and the numbers in January and February of the subsequent year (the numbers in January and February 1979 and in December 2005 are not included). Our purpose is to see if there are significant changes in the year-to-year observed seasonal heavy precipitation frequencies for the period of 1979–2005 and also if the analogue method can capture the interannual variations of these frequencies. We analyze the temporal trends in the observed seasonal heavy precipitation frequencies for all the regions and find that all the trends are not significantly different from zero at the 95% level. This is consistent with what was demonstrated in the previous studies (Mass et al. 2011; Kunkel et al. 1999). The analogue method is shown to represent the observed interannual variations of seasonal heavy precipitation frequencies rather well, especially for the WAOR. In particular, some large flooding events are successfully captured across various regions, including the 1993 Midwest flood (Fig. 7b); the well-documented widespread floods (and possible landslides) in 1981, 1994, 1995, 1996, and 1998 in Washington and Oregon (Fig. 7d); the floods in 1982, 1990 (plotted as 1989), 1991, and 1997 (plotted as 1996) in the south-central United States (Fig. 7a); and the floods in 1980 (plotted as 1979), 1982, 1986 (plotted as 1985), 1992, 1994, and 1996 in California (Fig. 7c). Compared with the MERRA precipitation, the analogue method clearly performs better with higher correlations and smaller RMSE against observations for all the regions.

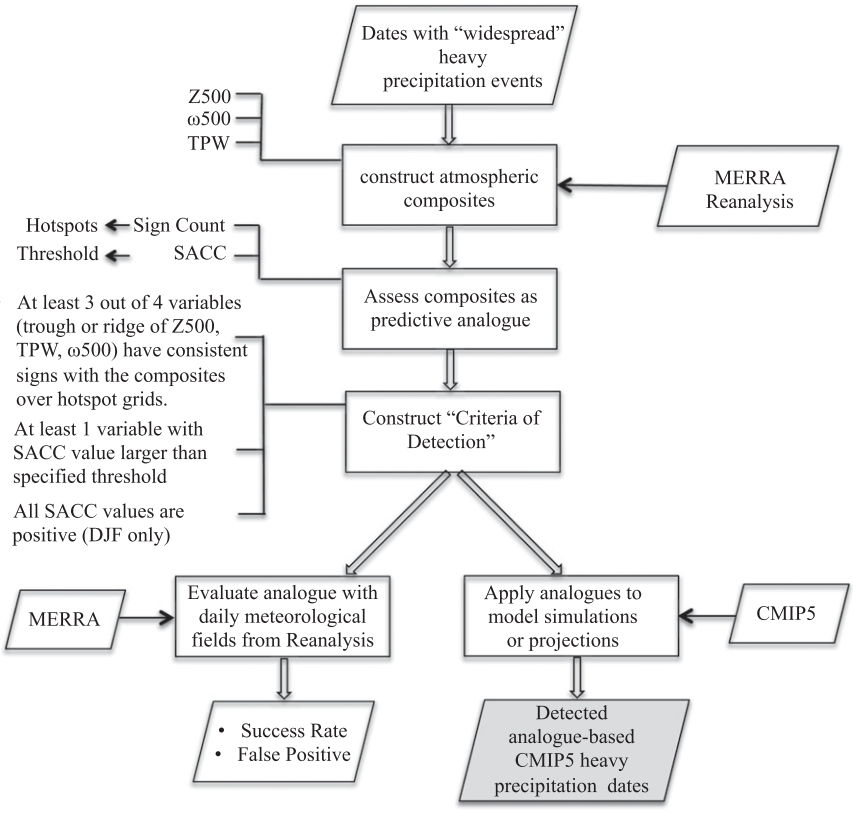

FIG. 8. A schematic diagram of the analogue method.

7. Application to CMIP5 historical model simulations

Next we apply the analogue method to the CMIP5 historical model simulations. We examine the capabilities of current state-of-the-art climate models to realistically simulate atmospheric dynamics and thermodynamics associated with heavy precipitation events and whether these events can be detected based on those resolved large-scale atmospheric conditions. This is achieved by comparing the CMIP5 model-simulated daily meteorological conditions with the constructed composites for their similarity in terms of the established criteria of detection. We want to know the following: how often will such large-scale composite patterns appear in the CMIP5 model simulations? Any day when criteria of detection are met would then be considered as having heavy precipitation events occurring. The schematic diagram of the analogue method is presented in Fig. 8. We compare the results using analogue approach with the heavy precipitation events identified from observations at 0.25° × 0.25°, MERRA precipitation, and the CMIP5 model-simulated precipitation at 2.5° × 2°. The heavy precipitation events identified from the precipitation observations aggregated to 2.5° × 2° are also presented in order to understand the effect of the spatial resolution. This also ensures that the results from the CMIP5 model-simulated precipitation are compared with the observed heavy precipitation events derived in a consistent manner.

a. Mean climate statistics

Figure 9 shows the comparisons of the total number of seasonal heavy precipitation events obtained from the CMIP5 model-simulated precipitation and the analogue method (applied to the CMIP5 model-simulated daily meteorological fields) across 20 climate models for the SCUS, PCCA, and WAOR in DJF as well as the MWST in JJA of 1979–2005. Also included are heavy precipitation events identified from the precipitation observations at 0.25° × 0.25° and 2.5° × 2° as well as MERRA precipitation.

The number of heavy precipitation events from the precipitation observations at two resolutions is close to each other for the SCUS (Fig. 9a). The analogue results that are based on the simulated large-scale atmospheric conditions of 20 CMIP5 models produce a more consistent number of heavy precipitation events with the

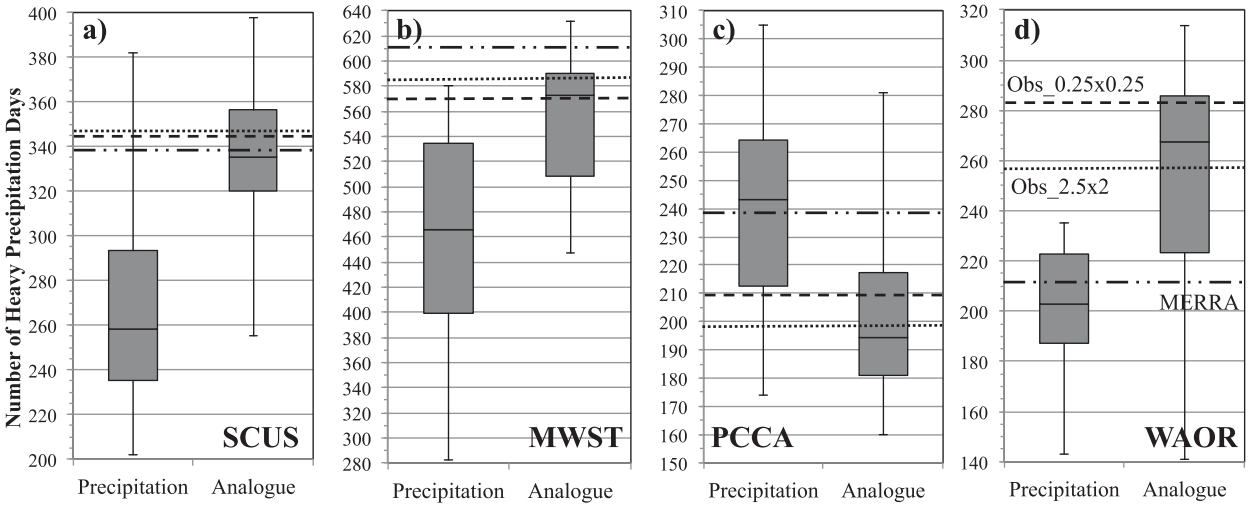

FIG. 9. Comparisons of the total number of seasonal heavy precipitation events estimated from CMIP5 model-simulated precipitation and CMIP5 analogues for the period 1979–2005 over our study regions. The whisker plot shows the minimum, the lower and upper quartile, the median, and the maximum across all 20 CMIP5 models. The dashed and dotted lines indicate the total number of heavy precipitation events widespread at the observation of 0.25° × 0.25° and identified from the observation at 2.5° × 2°, respectively. The dashed–dotted line indicates the total number of heavy precipitation events identified from MERRA precipitation at 2.5° × 2° (see text for further details).

observations. The analogue method also produces a reduced interquartile range (IQR) and total range across the climate models compared with the model-based precipitation. The central tendency (i.e., median) and IQR based on the CMIP5 model-simulated precipitation are significantly underestimated with the upper quartile even biased of about 50 days lower than the observation at 2.5° × 2°. In contrast, observed heavy event frequencies at both resolutions fall well within the IQR of the analogue results. MERRA precipitation captures the observed number of heavy event occurrences quite well. Overall, the analogue method improves upon the assessments of heavy precipitation frequency based on the model-simulated precipitation in terms of both accuracy and precision.

For the MWST, similar characteristics to the SCUS can be observed in Fig. 9b. It is evident that analogue-based heavy precipitation days across the models are more consistent with the observations and also less uncertain (smaller IQR and total range) than model-simulated precipitation. The median is rather close to the observations. The number of heavy precipitation days based on model-simulated precipitation is significantly underestimated with only one out of 20 models being close to the observation, while the MERRA precipitation overestimates the number of heavy precipitation days.

The comparisons of the total number of heavy precipitation days across all of the climate models from two schemes are shown in Fig. 9c for the PCCA. Again, the observed heavy precipitation days at two resolutions are quite comparable. Although the two schemes produce the similar total range of heavy precipitation days, the IQR that is statistically more robust than the total range is smaller for the analogue method. The analogue-based results are also more consistent with the observations at both resolutions, which are well bounded by the IQR. The precipitation-based analyses from the majority of models, however, overestimate the number of heavy precipitation days with the observations well beyond the lower quartile. Different from the SCUS region, MERRA precipitation is found to greatly overestimate the number of heavy precipitation days and align well with the median of the model-based precipitation analyses.

WAOR is the only region where the total number of heavy precipitation days based on the analogue method exhibits much larger IQR and total range across the models, almost double those from the precipitation-based analyses (Fig. 9d). Further examination suggests that such large ranges are mostly attributed to the significant underestimations by a set of L'Institut Pierre-Simon Laplace (IPSL) models (IPSL-CM5A-LR, IPSL-CM5A-MR, and IPSL-CM5B-LR) that only produce about half to two-thirds of the observations. Removal of these three models results in comparable IQR and total range to those of the precipitation-based analyses. Nevertheless, the median based on the analogue method is much more consistent with the observations that fall within the IQR. In contrast, the precipitation-based analyses significantly underestimate the total number of heavy precipitation days with the maximum

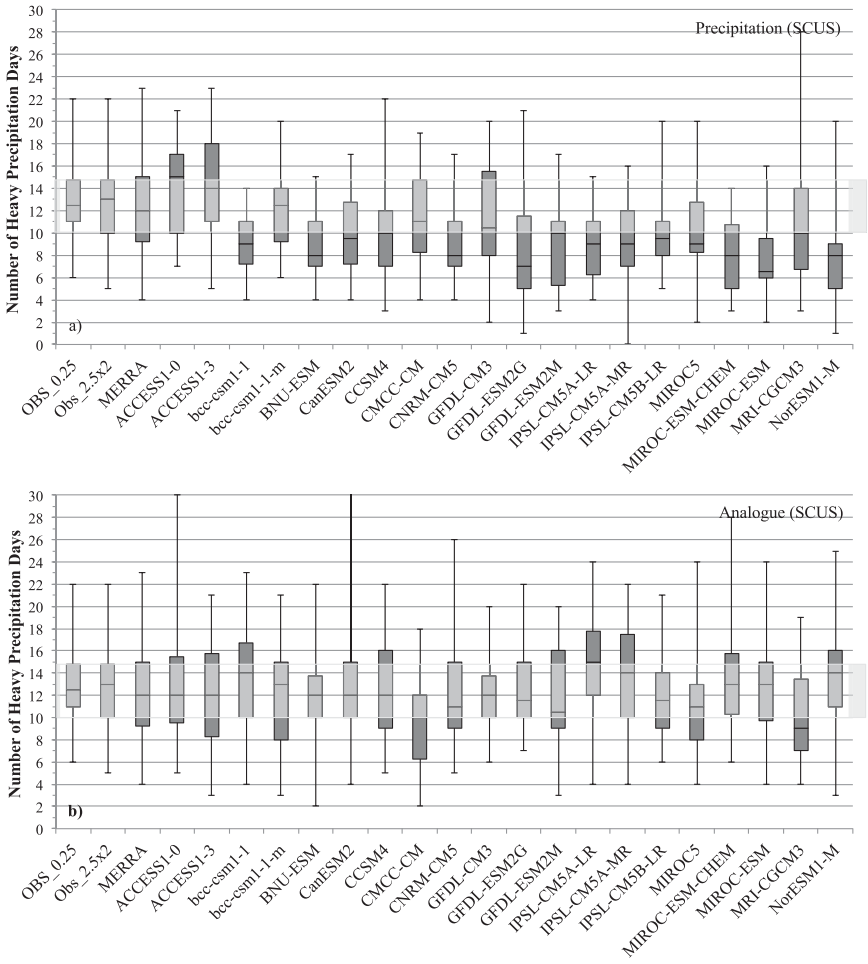

FIG. 10. Comparison of statistics for year-to-year seasonal heavy precipitation frequency obtained from (a) CMIP5 model-simulated precipitation and (b) CMIP5 analogues over the SCUS. The whisker plots display the minimum, lower and upper quartiles, median, and maximum of year-to-year seasonal heavy precipitation events during the 26-yr period (1979–2004). The OBS_0.25, OBS_2.5×2, and MERRA results are obtained from observation at 0.25° × 0.25° (widespread events), observation at 2.5° × 2°, and MERRA precipitation at 2.5° × 2°, respectively. Shaded gray areas represent the interquartile range (IQR) based on OBS_2.5×2.

still about 20 days lower than the observation. Substantial underestimation can be also seen in the MERRA precipitation result that aligns well with the median of the model-based precipitation analyses.

b. *Transient climate*

Because of the fundamental limits of deterministic predictability of the atmosphere, a comparison of seasonal heavy precipitation frequency for any particular year against observations is not an appropriate evaluation for the fully coupled historical CMIP5 simulations of the atmosphere–land–ocean system. Nevertheless, we can assess model-simulated variance against observations. We examine the statistics (minimum, lower and upper quartile, median, and maximum) for the year-to-year seasonal heavy precipitation frequencies from the analogue method and the CMIP5 model-based precipitation and further compare them with those from the observations and MERRA precipitation. To be consistent with how the heavy events are identified from the precipitation of the CMIP5 models and MERRA reanalysis, the statistics from the observation at 2.5° × 2° are used.

Figure 10 illustrates the 26-yr statistics computed from the observations, MERRA precipitation, and 20 CMIP5 model-simulated precipitation and large-scale atmospheric conditions (analogue method) for the SCUS region. The statistics from the observations at two resolutions are quite comparable to each other. We can also see that the analogue method and MERRA

TABLE 3. Rms error (units in number of heavy precipitation days) for statistics of year-to-year seasonal heavy precipitation frequencies between the analogue approach (Ana) as well as CMIP5 model-simulated precipitation (Prep) and precipitation observation at 2.5° × 2° over our study regions. The numbers in bold indicate that the statistics of the analogue method improve upon those of model-simulated precipitation.

	SCUS		MWST		PCCA		WAOR	
	Ana	Prep	Ana	Prep	Ana	Prep	Ana	Prep
Min	**1.55**	2.36	**3.26**	4.81	**1.16**	1.28	2.09	1.52
Q1	**1.47**	3.20	**3.20**	6.15	**1.76**	3.09	**1.18**	1.63
Median	**1.68**	3.93	**3.08**	6.04	**1.38**	1.92	**1.60**	2.06
Q3	**1.46**	3.26	**2.35**	4.74	**1.27**	2.09	2.34	2.33
Max	**3.99**	4.70	**10.66**	15.31	**6.02**	6.75	**4.58**	5.26

precipitation are both able to reproduce the statistics of the observation rather well. It is evident that the CMIP5 analogue results are more consistent with the observation than model-simulated precipitation, especially in terms of characterizing the IQR. The precipitation-based analyses reveal that the majority of the models tend to underestimate all the statistics for the year-to-year seasonal heavy precipitation days. To quantitatively evaluate the performances of two schemes, we compute the rms error (RMSE) of these statistics from two schemes against the observation across the 20 CMIP5 models (Table 3). The analogue results yield smaller RMSE than model-simulated precipitation for all the statistics, consistent with what is shown in Fig. 10.

The same analysis is presented in Fig. 11 for the MWST. Immediately evident is the improvement of the IQR characterizations exhibited by the analogue method over those by the model-simulated precipitation. The precipitation from the majority of the models tends to significantly underestimate all the statistics. The analogue results are more consistent with the observations with much smaller RMSE than modeled precipitation for all the statistics (Table 3). Worth to note is the largest RMSE in the maximum of the year-to-year seasonal heavy precipitation days exhibited by both schemes compared with other statistics. This is mostly attributed to the fact that both schemes, to some extent, fail to faithfully reproduce the large 1993 summer flood events across the study region. Nevertheless, the analogue method apparently performs collectively better in characterizing these hydrological extremes than model-simulated precipitation across various models.

For the PCCA, we can see that the IQRs of most models from the analogue method align well with observation, while the IQRs from the simulated precipitation of most models are clearly overestimated (Fig. 12). Extensive overestimation (19 out of 20 models) can also be seen in the maximum of the year-to-year seasonal heavy precipitation days. This is compatible with the mean statistics shown in Fig. 9c. Overall, the analogue results are more consistent with the observation than the precipitation-based analyses with the slightly smaller RMSE for all the statistics. Figure 13 shows the comparisons of the statistics from two schemes for the WAOR. In terms of the IQRs, model-simulated precipitation indicates the underestimations by almost all of the models, while analogue method suggests overall overestimations. In addition, we can clearly see that a set of IPSL models notably underestimate all the statistics, which is mostly responsible for the large spread in the total number of heavy precipitation days as shown in Fig. 9d. Compared with the observations, the analogue method improves over the model-simulated precipitation in characterizing most of the statistics, except for the minimum of the year-to-year seasonal heavy precipitation days (Table 3).

Some common features exist for all the regions that we examine here. The analogue approach is shown to outperform model-simulated precipitation by exhibiting a more consistent total number of heavy precipitation days with the observations and also smaller IQR across the models (except for the IQR in the WAOR). In terms of the statistics (minimum, lower and upper quartile, median, and maximum) for year-to-year seasonal heavy precipitation frequencies, the analogue method produces smaller RMSE against the observation for all the statistics across various regions, with the only exception being the minimum in the WAOR. However, both schemes seem to demonstrate difficulty in reproducing the maximum of the year-to-year seasonal heavy precipitation days for all the regions with the largest RMSE in comparison with other statistics. The better performance of the analogue method clearly suggests that current state-of-the-art climate models are capable of realistically simulating the atmospheric dynamics and thermodynamics associated with heavy precipitation events and, most importantly, with reasonable frequencies. This enables our analogue method, which is based on those resolved large-scale atmospheric conditions, to successfully detect the heavy precipitation events with improved mean and transient climate statistics over the model-simulated precipitation.

8. Summary and discussion

In this study, distinct large-scale atmospheric conditions that prevail during the occurrence of widespread heavy precipitation events at the local scale are diagnosed through the combined analyses of gridded finescale surface precipitation gauge observations and coarse-scale

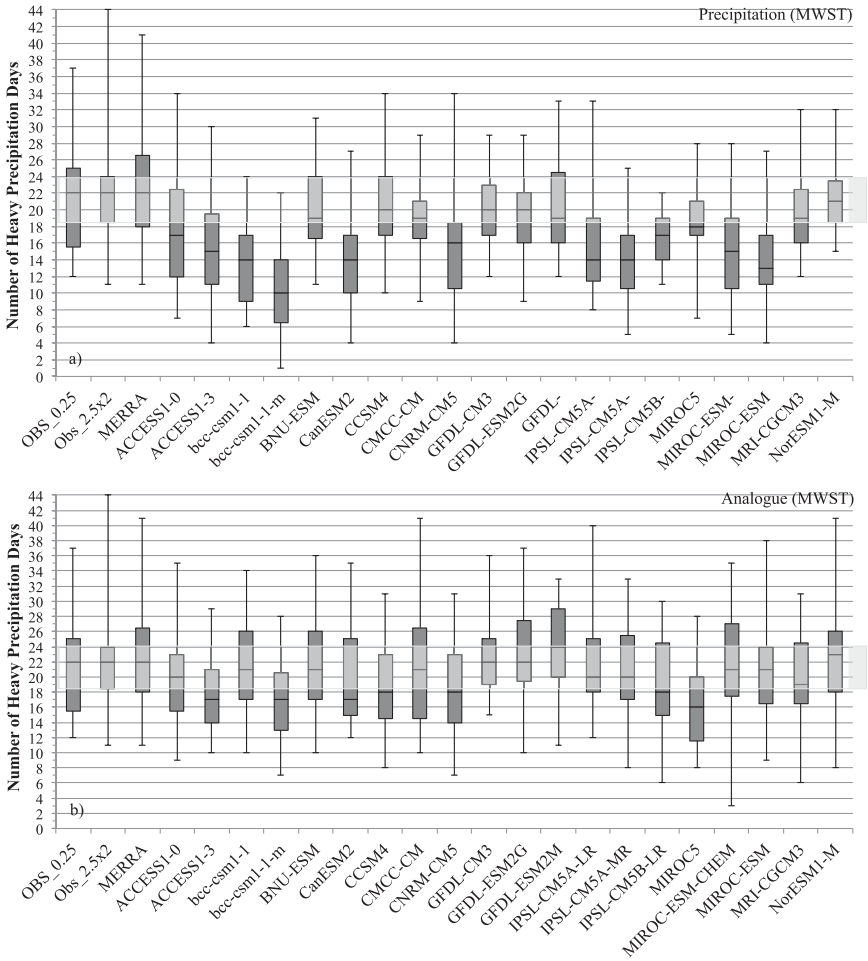

FIG. 11. As in Fig. 10, but for the midwestern United States (MWST) during the 27-yr period (1979–2005).

atmospheric reanalysis. The composites of such conditions are the derived mean flows, states, and fluxes from the reanalysis conditioned on the quantiles of surface precipitation observations. Nonparametric bootstrap scheme is employed to further constrain the quantile-formed conditioning state to ensure the widespread nature of localized heavy precipitation events and, thus, likely candidates for synoptic-scale association. Such procedure has several advantages, including 1) the composites are based on a pooled set of widespread heavy precipitation events that form a representative set of associated atmospheric conditions; 2) it is nonparametric in that the conditional average (composites) do not assume any distributions and is unbiased; and 3) it bridges the gap between the large-scale atmospheric conditions and local heavy precipitation. Our main objective is to examine whether the numerically resolved synoptic-scale atmospheric circulations of climate models can be used to identify the occurrence of heavy precipitation without relying on model-simulated precipitation, whose distributions in general do not accurately reproduce observations. In other words, can the diagnosed composites serve as predictive analogues for the occurrence of heavy precipitation?

We construct the composites from MERRA reanalysis for the winter season heavy precipitation in the south-central United States and U.S. West Coast as well as for the summer season in the midwestern United States. Various circulation features and moisture plumes associated with heavy precipitation are examined, including low-level flow (sea level pressure and wind), upper-level steering flow and dynamics (500-hPa geopotential height and 500-hPa vertical velocity), moisture flux, and total precipitable water. The identified synoptic regimes demonstrate interactions between low-level and upper-level flow fields and regional moisture supply. Composites in all the regions feature the presence of a dipole pattern associated with a pronounced trough

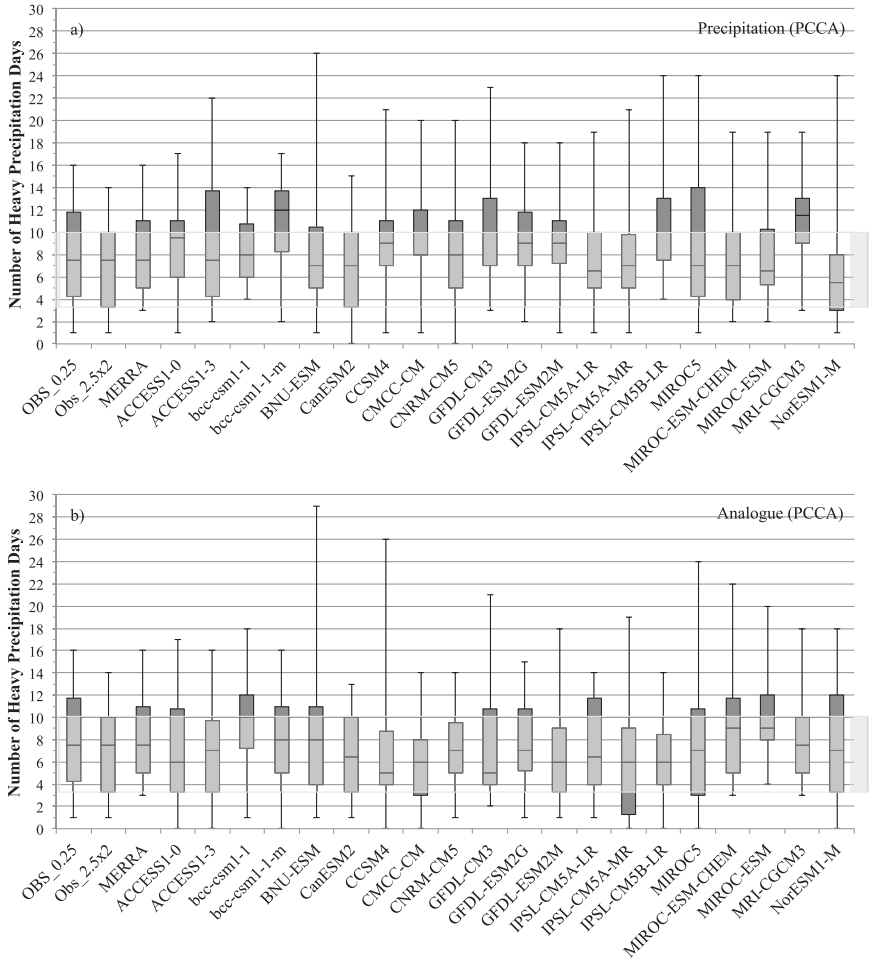

FIG. 12. As in Fig. 10, but for the California region (PCCA).

and a ridge over a much larger spatial scale as well as moist air and strong synoptic-scale upward motion directly over the study regions. Moisture transport for the south-central and the midwestern United States originates deeply from the Caribbean and extends from the Gulf of Mexico northward, exhibiting the characteristics of the Maya Express flood events. Moisture transport for the Pacific coast usually extends from the eastern North Pacific Ocean northeastward across the U.S. West Coast and exhibits the characteristics of the Pineapple Express flood events.

The development of the composite analogues for the occurrence of heavy precipitation is achieved by examining the sign consistency among the members of the composites and the spatial anomaly correlation coefficients (SACCs) between the MERRA daily atmospheric fields and the composites. Criteria of detection are then constructed such that a set of atmospheric conditions that support widespread, heavy precipitation are detected, based on 1) a selected group of grid cells where the sign are mostly consistent among the members of the composites and 2) the thresholds that differentiate between the distributions of the SACCs from heavy precipitation days and from the remaining days. The evaluation of the composite-analogue method based on the constructed criteria of detection with the MERRA daily meteorological fields demonstrates a success rate of around 80% and a false positive rate of about 20% in detecting the observed heavy precipitation events within one or two days. The analogue method is also shown to represent the observed interannual variations of seasonal heavy precipitation frequencies rather well with most of large flooding events in the historical period successfully captured across various regions.

The evaluation of the composite analogues in detecting heavy precipitation events from CMIP5 historical model simulations is made by examining how similar the model daily meteorological fields are to the composites in terms of the established criteria of detection. The results indicate that the analogue approach

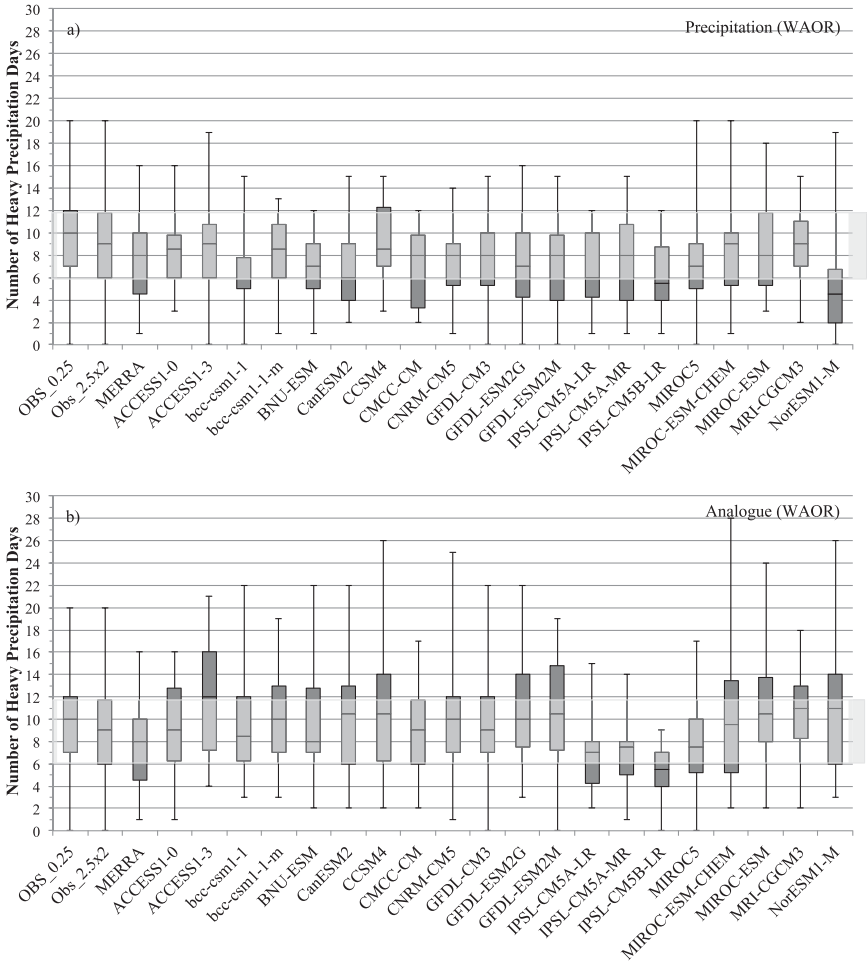

FIG. 13. As in Fig. 10, but for the Washington and Oregon region (WAOR).

produces more consistent total number of seasonal heavy precipitation days with what is observed and also smaller IQR across the models than the model-simulated precipitation over all the study regions. The simulated precipitation from the majority of the climate models significantly underestimates the total number of heavy events over the SCUS, MWST, and WAOR but overestimate it in the PCCA. In terms of representing the statistics (minimum, lower quartile, median, upper quartile, and maximum) for the year-to-year seasonal heavy precipitation frequency, the analogue approach is shown to outperform the model-simulated precipitation with smaller RMSE across all the models, except for the minimum in the WAOR. We also find that the analogue method and model-simulated precipitation both exhibit more difficulty in reproducing the maximum of the year-to-year seasonal heavy precipitation days in all the regions with the largest RMSE in comparison with other statistics. Overall, the analogue approach is shown to improve over the model-simulated precipitation in terms of characterizing the total number of and the statistics for year-to-year seasonal heavy precipitation days in the CMIP5 climate models. These results clearly suggest that global climate models are able to realistically simulate the large-scale atmospheric conditions associated with heavy precipitation events with the reasonable frequency. Accordingly, the analogue method developed in this study shows strong promise as a diagnostic tool to evaluate the representation of heavy precipitation events in climate models.

It should be pointed out that the analogue approach presented here is best used for characterizing the frequency but not the intensity of heavy precipitation. Returning to our original motivation for this study, we reconsider the questions posed in the introduction. Does the analogue approach based on resolved large-scale atmospheric features provide useful skill in detecting heavy precipitation events? Our results indicate the answer is yes. However, it should be noted that the specific details in the results of this investigation are almost

certainly dependent on the choices of many elements, such as the sign-consistency requirement and threshold values for SACCs. Although the physical mechanisms associated with heavy precipitation are generally well understood, the actual composites will vary with the seasonality as well as the location and size of the study region. As a result, the relevant meteorological recipes or criteria of detection for the occurrence of heavy precipitation would be also subject to adjustments. Nevertheless, the presented analyses highlight the improved diagnoses of the analogue approach against an evaluation that considers modeled precipitation alone to assess heavy precipitation event frequency. In principle, this analysis framework could be adapted to some other classes of extreme conditions (i.e., 99th or 99.5th percentile events), as well as over any region of interest, under the tested supposition that large-scale atmospheric conditions play a role. In this context, this analogue method and others like it could be extended to serve as a tool that bridges the gap between large-scale atmospheric conditions and local extreme environments of the natural and managed ecosystems, water resources, and air quality.

Acknowledgments. This work was funded by NASA Energy and Water Cycle Study Research Announcement (NNH07ZDA001N) and MacroSystems Biology Program Grant (NSF-AES EF#1137306) from the National Science Foundation. We acknowledge the modeling groups, the Program for Climate Model Diagnosis and Intercomparison (PCMDI), and the WCRP's Working Group on Coupled Modeling (WGCM) for their roles in making available the WCRP CMIP5 multimodel dataset. We thank the NOAA/Climate Prediction Center for the global gridded precipitation observations and the NASA Global Modeling and Assimilation Office for the MERRA reanalysis data. The authors gratefully acknowledge the comments received from Michael Bosilovich and two anonymous reviewers, which led to a substantially improved manuscript.

REFERENCES

Boroneant, C., G. Plaut, F. Giorgi, and X. Bi, 2006: Extreme precipitation over the Maritime Alps and associated weather regimes simulated by a regional climate model: Present-day and future climate scenarios. *Theor. Appl. Climatol.,* **86,** 81–99, doi:10.1007/s00704-005-0211-7.

Dai, A., 2006: Precipitation characteristics in eighteen coupled climate models. *J. Climate,* **19,** 4605–4630, doi:10.1175/JCLI3884.1.

DeAngelis, A. M., A. J. Broccoli, and S. G. Decker, 2013: A comparison of CMIP3 simulations of precipitation over North America with observations: Daily statistics and circulation features accompanying extreme events. *J. Climate,* **26,** 3209–3230, doi:10.1175/JCLI-D-12-00374.1.

Dirmeyer, P. A., and J. L. Kinter III, 2010: Floods over the U.S. Midwest: A regional water cycle perspective. *J. Hydrometeor.,* **11,** 1172–1181, doi:10.1175/2010JHM1196.1.

Groisman, P. Ya., and Coauthors, 1999: Changes in the probability of heavy precipitation: Important indicators of climatic change. *Climatic Change,* **42,** 243–283, doi:10.1023/A:1005432803188.

——, R. W. Knight, and T. R. Karl, 2001: Heavy precipitation and high streamflow in the contiguous United States: Trends in the twentieth century. *Bull. Amer. Meteor. Soc.,* **82,** 219–246, doi:10.1175/1520-0477(2001)082<0219:HPAHSI>2.3.CO;2.

——, ——, D. R. Easterling, T. R. Karl, G. C. Hegerl, and V. N. Razuvaev, 2005: Trends in intense precipitation in the climate record. *J. Climate,* **18,** 1326–1350, doi:10.1175/JCLI3339.1.

Grotjahn, R., 2011: Identifying extreme hottest days from large scale upper air data: A pilot scheme to find California Central Valley summertime maximum surface temperatures. *Climate Dyn.,* **37,** 587–604, doi:10.1007/s00382-011-0999-z.

Gutowski, W. J., S. G. Decker, R. A. Donavon, Z. Pan, R. W. Arritt, and E. S. Takle, 2003: Temporal–spatial scales of observed and simulated precipitation in central U.S. climate. *J. Climate,* **16,** 3841–3847, doi:10.1175/1520-0442(2003)016<3841:TSOOAS>2.0.CO;2.

——, S. S. Willis, J. C. Patton, B. R. J. Schwedler, R. W. Arritt, and E. S. Takle, 2008: Changes in extreme, cold-season synoptic precipitation events under global warming. *Geophys. Res. Lett.,* **35,** L20710, doi:10.1029/2008GL035516.

Hewitson, B. C., and R. G. Crane, 2006: Consensus between GCM climate change projections with empirical downscaling: Precipitation downscaling over South Africa. *Int. J. Climatol.,* **26,** 1315–1337, doi:10.1002/joc.1314.

Higgins, R. W., J.-K. E. Schemm, W. Shi, and A. Leetmaa, 2000a: Extreme precipitation events in the western United States related to tropical forcing. *J. Climate,* **13,** 793–820, doi:10.1175/1520-0442(2000)013<0793:EPEITW>2.0.CO;2.

——, W. Shi, E. Yarosh, and R. Joyce, 2000b: Improved United States precipitation quality control system and analysis. NCEP/Climate Prediction Center Atlas 7. [Available online at http://www.cpc.ncep.noaa.gov/products/outreach/research_papers/ncep_cpc_atlas/7/index.html.]

——, V. Silva, W. Shi, and J. Larson, 2007: Relationships between climate variability and fluctuations in daily precipitation over the United States. *J. Climate,* **20,** 3561–3579, doi:10.1175/JCLI4196.1.

——, V. E. Kousky, and P. Xie, 2011: Extreme precipitation events in the south-central United States during May and June 2010: Historical perspective, role of ENSO, and trends. *J. Hydrometeor.,* **12,** 1056–1070, doi:10.1175/JHM-D-10-05039.1.

Kharin, V. V., F. W. Zwiers, X. Zhang, and G. C. Hegerl, 2007: Changes in temperature and precipitation extremes in the IPCC ensemble of global coupled model simulations. *J. Climate,* **20,** 1419–1444, doi:10.1175/JCLI4066.1.

Klein Tank, A. M. G., F. W. Zwiers, and X. Zhang, 2009: Guidelines on analysis of extremes in a changing climate in support of informed decisions for adaptation. WMO/TD-1500, 56 pp.

Kunkel, K. E., K. Andsager, and D. R. Easterling, 1999: Long-term trends in extreme precipitation events over the conterminous United States and Canada. *J. Climate,* **12,** 2515–2527, doi:10.1175/1520-0442(1999)012<2515:LTTIEP>2.0.CO;2.

——, D. R. Easterling, K. Redmond, and K. Hubbard, 2003: Temporal variations of extreme precipitation events in the

United States: 1895–2000. *Geophys. Res. Lett.,* **30,** 1900, doi:10.1029/2003GL018052.

Lorenz, E. N., 1965: A study of the predictability of a 28-variable atmospheric model. *Tellus,* **17A,** 321–333, doi:10.1111/j.2153-3490.1965.tb01424.x.

Mass, C., A. Skalenakis, and M. Warner, 2011: Extreme precipitation over the West Coast of North America: Is there a trend? *J. Hydrometeor.,* **12,** 310–318, doi:10.1175/2010JHM1341.1.

Palmer, T. N., and J. Räisänen, 2002: Quantifying the risk of extreme seasonal precipitation events in a changing climate. *Nature,* **415,** 512–514, doi:10.1038/415512a.

Rienecker, M. M., and Coauthors, 2011: MERRA: NASA's Modern-Era Retrospective Analysis for Research and Applications. *J. Climate,* **24,** 3624–3648, doi:10.1175/JCLI-D-11-00015.1.

Rudari, R., D. Entekhabi, and G. Roth, 2004: Terrain and multiple-scale interactions as factors in generating extreme precipitation events. *J. Hydrometeor.,* **5,** 390–404, doi:10.1175/1525-7541(2004)005<0390:TAMIAF>2.0.CO;2.

——, ——, and ——, 2005: Large-scale atmospheric patterns associated with mesoscale features leading to extreme precipitation events in northwestern Italy. *Adv. Water Resour.,* **28,** 601–614, doi:10.1016/j.advwatres.2004.10.017.

Sun, Y., S. Solomon, A. Dai, and R. W. Portmann, 2006: How often does it rain? *J. Climate,* **19,** 916–934, doi:10.1175/JCLI3672.1.

Taylor, K. E., R. J. Stouffer, and G. A. Meehl, 2012: An overview of CMIP5 and the experiment design. *Bull. Amer. Meteor. Soc.,* **93,** 485–498, doi:10.1175/BAMS-D-11-00094.1.

Warner, M. D., C. F. Mass, and E. P. Salathé Jr., 2012: Wintertime extreme precipitation events along the Pacific Northwest coast: Climatology and synoptic evolution. *Mon. Wea. Rev.,* **140,** 2021–2043, doi:10.1175/MWR-D-11-00197.1.

Wehner, M. F., 2013: Very extreme seasonal precipitation in the NARCCAP ensemble: Model performance and projections. *Climate Dyn.,* **40,** 59–80, doi:10.1007/s00382-012-1393-1.

——, R. L. Smith, G. Bala, and P. Duffy, 2010: The effect of horizontal resolution on simulation of very extreme US precipitation events in a global atmosphere model. *Climate Dyn.,* **34,** 241–247, doi:10.1007/s00382-009-0656-y.